Precision Spectroscopy of Atomic Hydrogen

F. Biraben[1], T.W. Hänsch[2,3], M. Fischer[2], M. Niering[2], R. Holzwarth[2], J. Reichert[2], Th. Udem[2], M. Weitz[2,3], B. de Beauvoir[1], C. Schwob[1], L. Jozefowski[1], L. Hilico[1], F. Nez[1], L. Julien[1], O. Acef[4], J.-J. Zondy[4], and A. Clairon[4]

[1] Laboratoire Kastler Brossel, Ecole Normale Supérieure et Université Pierre et Marie Curie, CNRS UMR 8552, 4 place Jussieu, 75252 Paris Cedex 05, France
[2] Max-Planck-Institut für Quantenoptik, Hans-Kopfermann-Straße 1, D-85748 Garching, Germany
[3] Sektion Physik, Ludwig-Maximilians-Universität, Schellingstr. 4, D-80799 München, Germany
[4] Laboratoire Primaire du Temps et des Fréquences, BNM-Observatoire de Paris, 61 avenue de l'Observatoire, 75014 Paris, France

Abstract. We review advances in optical precision spectroscopy of atomic hydrogen achieved at Garching and Paris since the first symposium on the Hydrogen Atom at Pisa in 1988. The work at Garching has been focused on measurements of the $1S-2S$ and $2S-4S$ two-photon transitions in atomic hydrogen and on the isotope shift between hydrogen and deuterium. The Paris experiments have been directed at the $1S-3S$ and $2S-nS/nD$ transitions. A general least squares adjustment combining different measurements yields the currently most precise values for the Rydberg constant and the Lamb shift of the $1S$ ground state.

1 Introduction

Optical spectroscopy of hydrogen has played an important role since the beginnings of quantum physics because the simple hydrogen atom permits crucial confrontations of experiment and theory [1]. Doppler broadening limited classical spectroscopy to an accuracy of a few parts in 10^7. The advent of tunable lasers and nonlinear techniques of Doppler-free spectroscopy in the early seventies led to major advances in resolution and measurement precision [2]. At the time of the first Symposium on the Hydrogen Atom at Pisa in 1988, laser spectroscopic experiments in different laboratories had reached a precision of a few parts in 10^{10}, and they were approaching another formidable hurdle, the limits of optical wavelength interferometry, as imposed by unavoidable geometric wavefront errors.

Since then, hydrogen spectroscopy has inspired major advances in the art of measuring the frequency of light. With frequency interval divider chains [3], frequency comb generators [4,5] and other new tools, it has become possible to measure and compare hydrogen transitions to new levels of accuracy. These experiments have now yielded precise new values for the Rydberg constant, the Lamb shift of the $1S$ ground state, the charge radius of the proton, and the structure radius of the deuteron.

This article will review the spectroscopic experiments at Garching and Paris with emphasis on recent results. In Garching we have focused on measurements of the $1S-2S$ and $2S-4S$ two-photon transitions in atomic hydrogen and on the isotope shift between hydrogen and deuterium, as discussed in Section 2. In Paris, we have studied the $1S-3S$ and $2S-nS/nD$ transitions, as described in Section 3. Although both groups have independently determined values for the $1S$ ground state Lamb shift and the Rydberg constant, a general least squares adjustment combining these measurements yields the most precise results which are summarized in Section 4.

Right now, we are witnessing a dramatic change of paradigm in optical frequency metrology and precision spectroscopy. Femtosecond laser frequency comb techniques as pioneered in Garching have culminated in a compact and reliable single-laser frequency "chain" that permits the ultraprecise comparison of an optical frequency with the microwave frequency of a cesium atomic clock in a single step [6]. Precise optical frequency measurements are now, for the first time, within reach of small scale spectroscopy laboratories. We also have finally a "clockwork" that makes it feasible to construct more accurate atomic clocks based on sharp optical transitions in atoms, molecules, or ions. Future comparisons of different spectroscopic precision measurements are likely to test QED and fundamental symmetries to unprecedented levels. Such experiments may even unveil conceivable slow changes of fundamental constants or possible differences between matter and antimatter.

2 The Hydrogen $1S-2S$ Transition

For almost three decades, the $1S-2S$ transition in atomic hydrogen with its natural linewidth of only 1.3 Hz has inspired advances in high resolution laser spectroscopy, quantum electrodynamic theory, and optical frequency metrology [3,6]. With increasing accuracy of the transition frequency measurements, it was possible to determine new values for important physical constants [7]. In the future, conceivable slow changes of some fundamental constants might be revealed, and a comparison between hydrogen and antihydrogen will allow for a stringent test of CPT invariance for leptons and baryons [8].

2.1 Hydrogen $1S-2S$ Two-Photon Spectroscopy in an Atomic Beam

In 1990 an atomic beam spectrometer for Doppler-free continuous-wave two-photon spectroscopy of the hydrogen $1S-2S$ transition became first operational at Garching [9]. Its underlying principles had already been presented at the Pisa Symposium in 1988 [3]. In contrast to former experiments which measured this transition in a gas cell [10,11,12], the virtual absence of collisions in the atomic beam and the long interaction time between atoms and the excitation light due to the longitudinal geometry allowed measurements with several orders of magnitude increased accuracy. Fig 1 shows that apparatus in its present configuration [13,14].

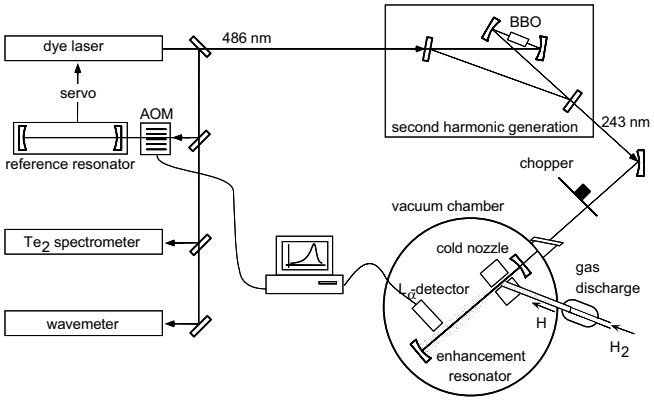

Fig. 1. Setup for Doppler-free two-photon spectroscopy of the hydrogen $1S-2S$ transition

A coumarin-102 dye laser pumped by a krypton ion laser emits about 500 mW radiation near 486 nm. Its frequency is servo locked to an external reference cavity by means of the Pound-Drever-Hall technique [15]. The reference cavity consists of two gyro-quality mirrors ($F \approx 57\,000$) optically contacted on a Zerodur spacer, which is suspended by soft springs inside a vacuum chamber. An acousto optic modulator (AOM) shifts the laser frequency to match one of the cavity modes. Fast frequency fluctuations of the dye laser are compensated for by an additional intracavity electro optic modulator (EOM). The blue light of this stable dye laser is resonantly enhanced in a ring cavity which is locked to the laser frequency [16]. In this cavity, a Brewster cut β-barium-borate crystal produces about 20 mW second harmonic light near 243 nm. After passing a mechanical chopper, the generated UV light is coupled into a linear enhancement cavity inside a vacuum chamber which is pumped by a 10 000 l/s cryopump. The cavity is locked to the second harmonic frequency by a second Pound-Drever-Hall lock.

Atomic hydrogen produced in a discharge outside the vacuum chamber is emitted collinearly to the axis of the enhancement cavity by a nozzle consisting of a small channel in a metal block. This geometry assures good overlap between the standing UV wave and the atomic trajectories, and long interaction times are possible. The block can be cooled, providing the opportunity to reduce the atomic beam temperature by collisions with the cold walls of the nozzle. After a distance of 15 cm over which the atomic beam is collinear with the UV standing wave, some atoms are excited to the $2S$ state by a Doppler-free two-photon transition. The atoms are then entering a $2S$ detector that uses a small dc electric quench field which mixes the $2S$ and the $2P$ states such that the excited atoms decay and emit a Lyman-α photon. This fluorescence is detected by a solar-blind photomultiplier tube. In order to reduce spurious background counts due to scattered 243 nm radiation, the light field is chopped, and signal photons are detected only during the dark times. A computer is used to control the AOM frequency and to record the data.

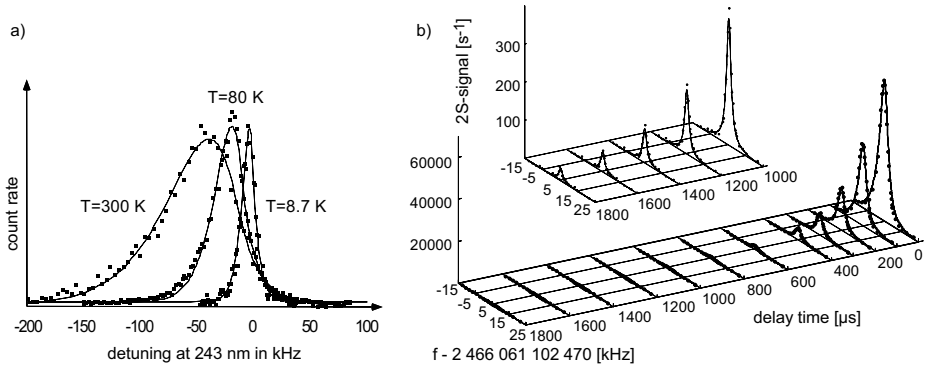

Fig. 2. Doppler-free spectra of the $1S-2S$ two-photon transition ($F=1 \rightarrow F=1$) in atomic hydrogen. a) Spectra for three different nozzle temperatures and no delay time. b) Time resolved spectrum (nozzle temperature 6.5 K). This plot gives the $2S$ count rate as a function of the absolute optical frequency for different delay times. The inset shows the spectra with longer delay times on a magnified scale

With this experiment, it became possible to observe the Doppler-free two-photon $1S-2S$ resonance in a hydrogen atomic beam. At an atom temperature of roughly 170 K obtained by cooling the nozzle with liquid nitrogen, the measured linewidth was 60 kHz at 243 nm, corresponding to a resolution of 5 parts in 10^{11}. It was limited by the second order Doppler effect ($\approx$ 25 kHz) and time of flight broadening. In subsequent experiments, the spectral resolution was significantly improved, mainly by the use of a copper nozzle cooled with a liquid helium cryostat, so that the temperature of the beam was reduced to 7 K. Spectra taken at different temperatures clearly show the decrease of the linewidth with lower temperatures (Fig. 2 a)). Noticeably, the second order Doppler shift ($\propto v^2/c^2$), causing an asymmetry of the spectra, decreases faster for lower temperatures than the time of flight broadening ($\propto v$). The second order Doppler shift gives not only a line broadening, but also a systematic redshift of the line center.

In later measurements, very slow atoms from the broad Maxwellian velocity distribution were selected in order to allow for even narrower lines and smaller systematic shifts. For these measurements, the signal detection was enabled only at a (variable) delay time τ after blocking the excitation light field with the chopper, such that only atoms with velocities v below $v_{max} = d/\tau$ (d being the distance between nozzle and photomultiplier) could contribute to the signal. The drastically reduced count rate at high delay times, however, makes data analysis difficult. Therefore, a multichannel photon counter is now used to register all signal photons tagged with their arrival times. An example for a recent time resolved measurement is shown in Fig. 2 b).

The transit time broadening has been further reduced by installing a small aperture in front of the photomultiplier. Thereby, only atoms that travel close to the axis of the enhancement cavity contribute to the signal.

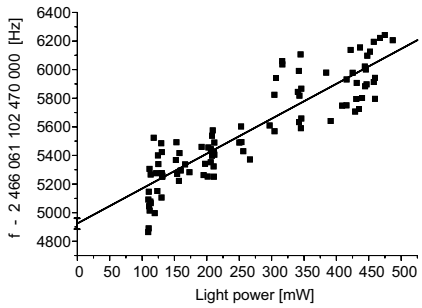

Fig. 3. Absolute $1S-2S$ transition frequencies ($F=1 \rightarrow F=1$ component) derived from the line shape model and plotted versus excitation light power

2.2 Theoretical Line Shape Model

For an accurate data analysis, a detailed understanding of systematic effects is necessary. Although they are significantly reduced with the improved spectroscopy techniques described above, they still broaden the absorption line profile and shift the center frequency. In particular, the second order Doppler shift and the ac-Stark shift introduce a displacement of the line center. To correct for the second order Doppler shift, a theoretical line shape model has been developed which takes into account the geometry of the apparatus as well as parameters concerning the hydrogen atom flow. The model is described in more detail in Ref. [13].

By numerical integration of the Bloch equations describing the classical trajectory of an atom from the nozzle through the standing wave field at 243 nm to the detector and integration over all possible trajectories and over the velocity distribution of the atoms, a theoretical line shape is deduced which is then fitted to the experimental data. The solid lines in Fig. 2 are obtained from this fitting procedure.

A single set of seven parameters is sufficient to fit all velocity classes simultaneously, which means that not only the counts from slow atoms but all counts are used to find the true line center. The parameters are: a universal amplitude of the measured line profile, the laser detuning which describes the difference between measured and unperturbed line center, the slightly modified Maxwellian-like velocity distribution of the atoms modelled by three parameters, the beam temperature and the linewidth of a Lorentzian profile folded in which takes care of additional broadening effects like the linewidth of the laser. In this way, the second order Doppler shift is corrected for within ≈ 20 Hz. We account for the ac-Stark shift by recording spectra at different light intensities and extrapolating the resulting line centers to zero laser power, as shown in Fig. 3. With the Garching line shape model, it has been verified that the shift is, as predicted, linearly dependent on the intensity with a slope that is in good agreement with the theory.

2.3 Optical Lamb Shift Measurements

In initial experiments at Garching we have combined the $1S-2S$ spectrometer with another atomic beam apparatus for the excitation of the $2S-4S/4D$ transition in atomic hydrogen similar to the experiments in Paris [17,18,19], aiming at an improved measurement of the hydrogen ground state Lamb shift $L(1S)$ [20].

By comparison of one quarter of the $1S-2S$ transition frequency with the $2S-4S$ and $2S-4D$ transition frequency, the main energy contributions described by the simple Rydberg formula are eliminated. The remaining difference frequency (about 5 GHz) is determined by well known relativistic contributions, the hyperfine interaction, and a combination of Lamb shifts. Since quantum electrodynamic contributions scale roughly as $1/n^3$ with the principal quantum number, the Lamb shift of the $1S$ level is the largest.

The discovery of the $2S-2P$ Lamb shift has led to the development of the theory of quantum electrodynamics. Today, radio frequency measurements of this splitting have reached the uncertainty limits imposed by the 100 MHz natural linewidth of the $2P$ state. The considerably sharper optical two-photon resonances used in optical experiments leave significant room for future improvements.

To excite the $2S-4S/4D$ two-photon transition a Ti:Sapphire laser operating near 972 nm is used. The laser is locked to a stable reference cavity using a piezo mounted mirror and an external AOM to compensate for fast frequency fluctuations. A second AOM allows the tuning of the laser over the atomic resonance. The light is coupled into an external longitudinal enhancement cavity built around the $2S-4S$ vacuum chamber similar to the $1S-2S$ apparatus. However, here metastable $2S$ atoms are created by electron impact and are directed onto the laser axis as shown in Fig. 8. After an interaction region which is collinear with the standing laser wave, the remaining atoms in the $2S$ state are detected in a similar way as described by the Paris group in section 3.1. A $2S-4S/4D$ two-photon excitation leads to a decreased $2S$ count rate, as the excited atoms reach the $1S$ ground state via an intermediate P state with 95 % probability. The typical observed decrease in the metastable yield was 5 % for the $2S-4S$ spectra, and 20 % for the $2S-4D$ spectra.

A small part of the infrared light was frequency doubled in a $KNbO_3$ crystal to 486 nm and combined with the blue light of the dye laser that excites the $1S-2S$ transition. A fast photodiode is used to observe the frequency difference $\nu(2S-4S/4D)-1/4*\nu(1S-2S)$. Fitting the $2S-4S$ and $2S-4D$ line profiles with a theoretical model calculated by Garreau *et al.* [17,18,19] and correcting for some systematic effects, the ground state Lamb shift could be determined with an accuracy of 1.3 parts in 10^5, one order of magnitude more precise than in previous measurements [21,22].

Two years later, a detection system for Balmer-β fluorescence was added to the $2S-4S/4D$ apparatus. Because of the better signal to noise ratio of that signal a remeasurement for both hydrogen and deuterium [23] resulted in improved values. By that time, the relative precision of the $1S$ Lamb shift already exceeded that of radio frequency measurements of the classic $2S-2P$ Lamb shift.

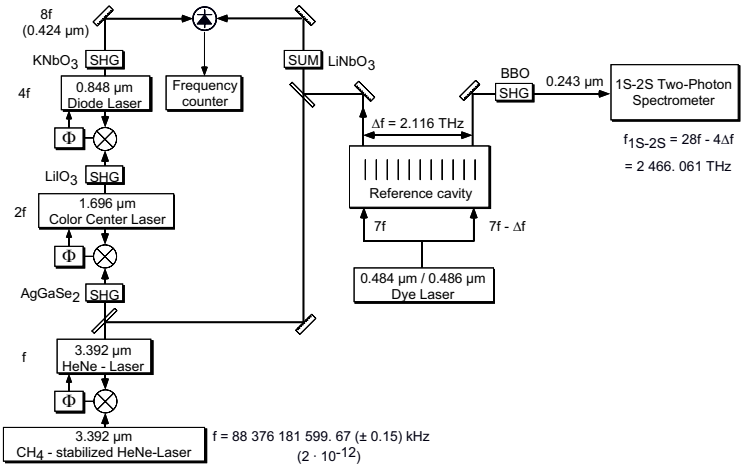

Fig. 4. The first 1992 Garching frequency chain for the measurement of the $1S-2S$ transition in atomic hydrogen (Φ: phase-locked loop, SHG: second harmonic generation)

An even more accurate value of the $1S$ Lamb shift can now be derived from a comparison of absolute frequency measurements of the $1S-2S$ and $2S-nS, nD$ transitions in Garching and Paris, as discussed in Section 3–4.

2.4 Absolute Measurements of the $1S-2S$ Transition Frequency in Atomic Hydrogen

Until 1992, the accuracy of spectroscopic measurements was limited to 1.6 parts in 10^{10} by the reproducibility of the I_2-stabilized HeNe laser at 633 nm which served as an optical frequency standard, and by the unavoidable geometric wavefront errors in wavelength interferometry. To overcome this limitations it was necessary to measure the optical frequency rather than the wavelength.

The first frequency measurement of the $1S-2S$ resonance made use of a transportable CH_4-stabilized HeNe infrared frequency standard at 88 THz [24], built at the Institute of Laser Physics in Novosibirsk/Russia. For calibration it was transported repeatedly to the Physikalisch-Technische Bundesanstalt (PTB) in Braunschweig/Germany where it could be compared with a Cs atomic clock using the PTB frequency chain [25].

The first Garching laser frequency chain shown in Fig. 4 takes advantage of the near coincidence between the 28th harmonic of the CH_4-stabilized HeNe laser frequency $28f$ and the $1S-2S$ transition frequency in atomic hydrogen being $28f-4\Delta f$. With three frequency doubling stages, the 8th harmonic of the fundamental frequency at 424 nm was generated. When combining that frequency with the sum of the dye laser frequency at $7f-\Delta f$ and the frequency of the HeNe standard f on a photodiode, a beat signal of Δf could have been observed in principle. However, as $\Delta f \approx 2.116$ THz and no fast counting technique was

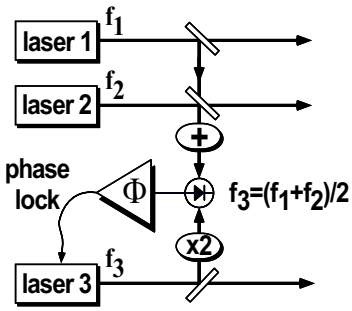

Fig. 5. Principle of an optical frequency interval divider. An arbitrary large frequency interval $f_1 - f_2$ is phase coherently divided by two by locking a third laser (f_3) precisely in the center of the interval. This is achieved by phase locking the sum frequency $f_1 + f_2$ to the second harmonic $2f_3$. Then $f_3 = (f_1 + f_2)/2$ holds

available at that time, the dye laser was alternately locked to two modes of the reference cavity, one close to the fourth subharmonic of the $1S - 2S$ transition ($7f - \Delta f$) and the other at $7f$ as obtained from the sum frequency $7f + f = 8f$ as shown in Fig. 4. The $1S - 2S$ transition frequency was then determined from the calibrated HeNe laser (f) and the measured frequency difference Δf obtained by counting the number of reference cavity modes needed to bridge the gap. The mode spacing was precisely measured beforehand with the help of a 84 GHz EOM [26]. The obtained accuracy of 1.8 parts in 10^{11} represented an 18-fold improvement, limited then by the interpolation of the cavity drift.

The next big advance towards higher precision was the 1997 phase-coherent measurement of the frequency gap with an optical frequency interval divider chain [27]. The 2.1 THz gap was no longer measured by counting cavity fringes, but divided down to the radio frequency domain by a phase-locked chain of five optical frequency interval dividers [56] (see Fig. 5). The accuracy of this approach was limited by the secondary frequency standard to 3.4 parts in 10^{13}, exceeding the accuracy of the best previous measurements by almost two orders of magnitude.

The most recent absolute measurement of the hydrogen $1S - 2S$ transition frequency [28] took advantage of the revolutionary femtosecond comb technology discussed in detail elsewhere in this volume [6]. We shall therefore describe this technique only briefly. The first direct link between an ultraviolet optical frequency and the microwave frequency of a cesium atomic clock has been achieved with the use of a femtosecond laser frequency comb using a modified version of the existing Garching frequency chain, as sketched in Fig. 6. From the dye laser for the excitation of the $1S - 2S$ resonance, two optical frequencies $4/7 f_{dye}$ and $1/2 f_{dye}$ are derived. While the first frequency involved the frequency chain shown in the left part of Fig. 4, the second frequency is generated by phase locking the second harmonic of a diode laser near 972 nm to the dye laser. The frequency gap between $4/7 f_{dye}$ and $1/2 f_{dye}$, corresponding to 44 THz, is sufficiently small

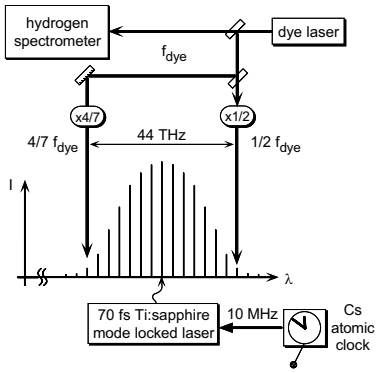

Fig. 6. Comparison of the hydrogen $1S-2S$ transition frequency with a Cs clock using a femtosecond comb. This is a simplified version of the frequency chain shown in Fig. 4 Ref. [6] in this volume

that it can be measured with the wide comb of regularly spaced modes emitted by a mode-locked fs laser. The mode spacing is given by the repetition rate of the fs laser, which is phase locked to a Cs atomic clock.

We wish to point out, that by use of a suitable fiber which further broadens the spectrum, this fs laser frequency measurement technique has now been simplified to a setup with a single laser, as described elsewhere in this volume [6]. With the technique of Fig. 6, the $1S-2S$ transition frequency was measured twice, first with a GPS referenced commercial Cs clock [29], and second with a transportable Cs atomic fountain clock constructed by A. Clairon and coworkers in Paris [30]. A total of 614 spectral lines was recorded in the latter measurement during ten days, and fitted with the described line shape model [13]. After adding a correction of 310 712 233(13) Hz to account for the hyperfine splitting of the $1S$ and $2S$ levels, we obtain for the hyperfine centroid [28]:

$$\nu(1S-2S) = 2\ 466\ 061\ 413\ 187\ 103(46)\ \text{Hz}$$

This measurement represents now the most precise measurement of an optical frequency, and the best realization of the meter.

2.5 $1S-2S$ Isotope Shift and the Deuteron Structure Radius

The deuteron, being the simplest compound nucleus, provides an important testing ground for theories of nuclear few body systems which predict the deuteron structure radius. Traditionally, this radius has been determined from accelerator-based electron scattering data. In an optical spectroscopy experiment in 1993, a new value for the deuteron structure radius with significant deviation from the previously adopted value was found [31].

We focus here on the description of the 1997 measurement of the hydrogen-deuterium $1S-2S$ isotope shift carried out in Garching [32], that confirmed

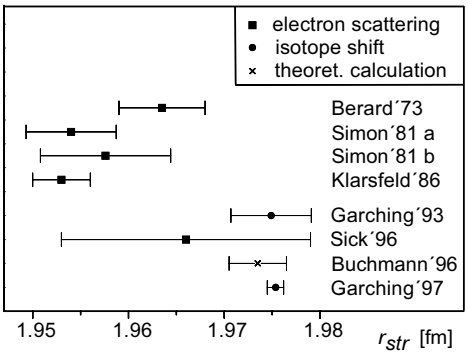

Fig. 7. Values for the deuteron structure radius

the 1993 result. A passive comb generator was used to measure the frequency difference of 671 GHz between the $1S-2S$ transition in hydrogen and deuterium. This comb generator [4,5] consisted of a single crystal passive optical resonator that is used as an efficient electro optic modulator to impose sidebands on an injected cw laser. At that time the achievable spectral width was limited by the crystal group velocity dispersion to a few THz [4]. External optical amplification with subsequent self-phase modulation in an optical fiber could today surpass that limit [33]. After applying gain to a passive modulator and compensating for the group velocity dispersion, the use of a mode-locked laser is just the consequential continuation of this technology.

The Garching group obtained an experimental result for the $1S-2S$ transition frequency isotope shift of 670 994 334.64(15) kHz, from which one also can calculate a value for the deuterium $1S-2S$ transition frequency: $\nu(1S-2S) =$ 2 466 732 407 521.74(16) kHz [32]. Most of the H-D isotope shift is caused by the different recoil/masses of the nuclei. The leading term is obtained by calculating the difference of the transition frequencies from the Dirac energies $R_\infty e(nl)$ that include all mass dependent recoil corrections up to the order $(Z\alpha)^4$ [34]. The resulting value already agrees with the observed value within 1.4×10^{-5}. The remainder belongs to the Lamb shift of the corresponding levels which include a nuclear size dependent contribution. The complete calculation of the isotope shift *without* the size dependent terms yields 670 999 569.1(1.6) kHz [35]. In subtracting this from the measured value, one obtains a frequency that is proportional to the difference of the mean square charge radii with a known coefficient [32], yielding

$$r_{d,ch}^2 - r_{p,ch}^2 = 3.821\,5(12)\ \mathrm{fm}^2.$$

The deuteron structure radius can be written as $r_{d,str}^2 = (r_{d,ch}^2 - r_{p,ch}^2) - r_{n,ch}^2 - 3/(4\,m_p^2)$ [38], where $r_{n,ch}^2 = -0.114(3)\ \mathrm{fm}^2$ [39] is the neutron charge radius and m_p is the proton mass. From this equation one can derive a deuteron structure radius of

$$r_{d,str} = 1.975\,44(82)\ \mathrm{fm}$$

in agreement with a theoretical determination $r_{d,str} = 1.9735(30)$ fm [38]. The currently most precise value obtained from electron scattering [40] ($r_{d,str} = 1.953(3)$ fm) however disagrees by more than seven combined standard deviations. A summary of published values for the deuteron structure radius is shown in Fig. 7 [41,42,40,31,43,38].

The precision of this atomic table top measurement exceeds the accuracy of previous measurements based on elastic electron scattering by an order of magnitude. The reanalysis of electron scattering data by Sick and Trautmann [43] yields a value with an increased uncertainty, which is in good agreement with the data obtained in the Garching experiment.

3 Spectroscopy of the $2S - nS$ and $2S - nD$ Transitions

3.1 Method

The principle of the Paris experiment is described in the references [17,18,19]. The experimental geometry is illustrated in Fig. 8. A metastable atomic beam is formed by electronic excitation of a $1S$ hydrogen atomic beam. Due to the inelastic collision with the electron, the atomic trajectory is deviated by an angle of about 20°. The deviation is used to make the $2S$ atomic beam collinear with the laser beams after the collision. This geometry reduces the transit time broadening. The metastable yield is monitored at the end of the atomic beam: an electric field quenches the metastable state and two photomultipliers detect the Lyman-α fluorescence. The two-photon transition is induced with a highly stable titanium-sapphire laser (the frequency jitter is reduced to the level of 2 kHz). The atomic beam is placed inside an enhancement cavity, where the optical power can be as much as 100 W in each direction. When the laser frequency is in resonance with the $2S - nS/D$ transition, the atoms in the nS or nD states undergo a radiative cascade towards the $1S$ state in a proportion of about 95 %. The optical quenching of the metastable level occurs before the detection region, and the optical excitation can be detected via the corresponding decrease of the 2S beam intensity.

Figure 9 shows a typical signal obtained for the case of the $2S_{1/2}(F = 1) - 8D_{5/2}$ (the hyperfine structure of the $8D_{5/2}$ level is not resolved) transition of deuterium. In this recording, the decrease of the metastable intensity is 18 % and the linewidth is 2 MHz (in terms of atomic frequency). By comparison with the natural width of the $8D$ level (572 kHz), there is a large broadening which is mainly due to the inhomogeneous light shift experienced by the atoms through the gaussian profile of the laser beams. To evaluate this effect, the signal is recorded for several laser intensities and the line position is extrapolated to zero light power. For each recording, a theoretical profile is fitted to the experimental curve. This theoretical line shape takes into account the light shift, the saturation of the transition, the small hyperfine structure of the D levels, the photoionization, the small deviation of the atomic trajectories due to the light forces, as well as the second order Doppler shift. The velocity distribution is measured by monitoring the Doppler shifted $2S-6P$ transition. Each fit gives

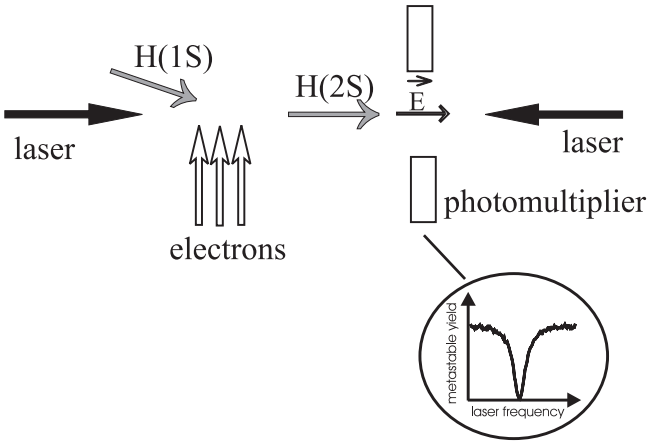

Fig. 8. Experimental geometry of laser and atom beams to observe the $2S - nS$ and $2S - nD$ two-photon transitions. When the laser frequency is scanned over the resonance, we observe a decrease of the metastable yield (see the inset)

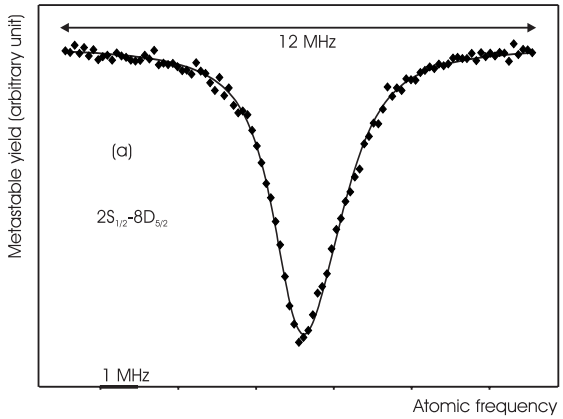

Fig. 9. Fit of the experimental line profile with the theoretical one for the $2S_{1/2}(F = 1) - 8D_{5/2}$ transition in deuterium. The light power deduced from the fit is 90.6(2.2) W and the decrease of the metastable yield is 18 %

both the experimental line center and the line position corrected for the light shift, the hyperfine structure of the D level and the second order Doppler effect. An extrapolation of these data is given in Fig. 10.

3.2 Optical Frequency Measurements in Paris

In 1988, the Paris group carried out an interferometric measurement of the $2S_{1/2} - 8D_{5/2}$, $2S_{1/2} - 10D_{5/2}$ and $2S_{1/2} - 12D_{5/2}$ transitions in hydrogen and

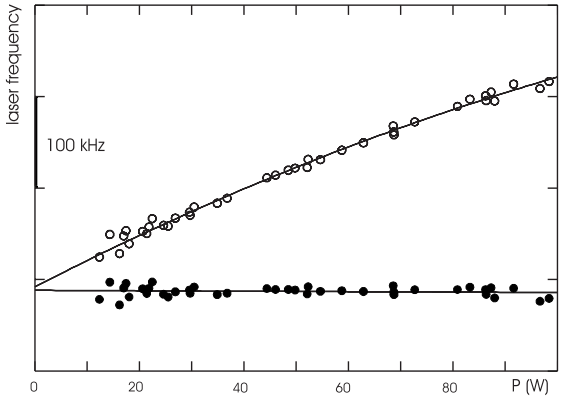

Fig. 10. Extrapolation of the half maximum center (○) and of the line position corrected for the light-shift, second order Doppler effect and 8D hyperfine structure (●) versus the light power P in the case of the $2S_{1/2}(F=1)-8D_{5/2}$ transition of deuterium

deuterium with respect to an iodine stabilized He-Ne laser [44,10]. These measurements provided a determination of the Rydberg constant with an accuracy of 1.7×10^{-10}. In the last decade, the optical frequency measurements have superseeded the interferometric ones. In Paris, the optical frequencies of the $2S_{1/2} - 8S_{1/2}$, $2S_{1/2} - 8D_{3/2}$ and $2S_{1/2} - 8D_{5/2}$ transitions in hydrogen were measured in 1993 with a frequency chain using two standard lasers (the iodine stabilized and the methane stabilized helium-neon lasers). The precision was in the range of 10^{-11} [45,46]. In 1996, these measurements were remade in hydrogen and deuterium with an accuracy better than one part in 10^{11} [47]. A new frequency chain was used with a new standard laser, namely a diode laser at 778 nm stabilized on the $5S_{1/2} - 5D_{5/2}$ two-photon transition of rubidium (LD/Rb laser). The frequency of this standard was measured with a frequency chain at the *Laboratoire Primaire du Temps et des Fréquences* (LPTF) [48]. More recently, in order to check these $2S - 8S/D$ frequency measurements, a new chain has been built to measure the frequencies of the $2S - 12D$ transitions in hydrogen and deuterium [49]. These experiments are described in detail in reference [50].

The cornerstone of the recent optical frequency measurements in Paris is the LD/Rb standard laser [51,52,53]. Three identical systems have been built, two at the LPTF and a third in *Laboratoire Kastler Brossel*. As the two laboratories are linked by two 3 km long optical fibers, it is possible to compare the frequencies of the three systems. The frequency shift due to the fiber has been checked with the highly stabilized titanium-sapphire laser. After a round trip of 6 km through the fibers, a maximum frequency shift of 3 Hz is observed [54]. This shift is completely negligible for the optical frequency measurements. The main metrological features of the LD/Rb laser are a frequency stability (Allan variance) of about $4 \times 10^{-13}\tau^{-1/2}$ per laser over 1000 s and a day-to-day repeatability of 400 Hz.

The frequencies of the three LD/Rb lasers stabilized on the $5S_{1/2}(F = 3) - 5D_{5/2}(F = 5)$ two-photon transition of ^{85}Rb were measured in 1996. The LPTF frequency chain connects the LD/Rb laser at 385 THz to a standard at 29 THz, namely a CO_2 laser stabilized to an osmium tetraoxyde line (CO_2/OsO_4) [48]. This standard had been previously measured in 1985 with respect to the Cs clock with an uncertainty of 70 Hz. In 1998, the measurement of the CO_2/OsO_4 standard was remade with an uncertainty of 20 Hz (*i.e.* a relative uncertainty of 7×10^{-13}) [55]. Taking into account this last measurement, the frequency of the LD/Rb standard of LKB is, after correction of the light shift: $\nu_{KB} = 385\ 285\ 142\ 376.7(1.0)$ kHz.

Table 1. Experimental determination of the $2S - 8S/D$ transition frequencies from the measurements made in hydrogen with the rubidium standard. All the values are in MHz and we have subtracted a frequency ν_0 of 770 649 GHz

Transition in hydrogen	$2S_{1/2} - 8S_{1/2}$	$2S_{1/2} - 8D_{3/2}$	$2S_{1/2} - 8D_{5/2}$
Result of extrapolation $-\nu_0$	306.3175(70)	460.0609(66)	517.1958(40)
Stark effect	-0.0006(4)	0.0005(3)	-0.0002(1)
Black body radiation	-0.0005(1)	-0.0006(2)	-0.0006(2)
$2S_{1/2}$ hyperfine shift	44.3892	44.3892	44.3892
$8S_{1/2}$ hyperfine shift	-0.6936		
$\nu(2S_{1/2} - 8S_{1/2}/8D_J) - \nu_0$	350.0120(86)	504.4500(83)	561.5842(64)
$8S_{1/2}/8D_{3/2} - 8D_{5/2}$ splitting	211.5621	57.1291	
$\nu(2S_{1/2} - 8D_{5/2}) - \nu_0$	561.5741(86)	561.5791(83)	561.5842(64)
Mean value and χ^2	770 649 561.5811(59)		$\chi^2 = 1.69$

The frequency comparison between the $2S-8S/D$ transitions and the LD/Rb standard laser is easy, thanks to the quasicoincidence between these frequencies. We have: $\nu(2S - 8S/D) = \nu(LD/Rb) + \Delta$, where the residual difference Δ is about 40 GHz in hydrogen and 144 GHz in deuterium. This frequency difference is measured with a Schottky diode. The $2S_{1/2} - 8S_{1/2}$, $2S_{1/2} - 8D_{3/2}$ and $2S_{1/2} - 8D_{5/2}$ two-photon transitions in hydrogen and deuterium have been measured with this method. Table 1 gives the analysis of the results for hydrogen with the corrections due to the Stark effect, the black body radiation and the hyperfine structure. The three experimental values of the $2S_{1/2} - 8S_{1/2}$ and $2S_{1/2} - 8D_J$ splittings can be intercompared using the theoretical values of the fine structure and of the Lamb shifts in the $n = 8$ levels. The three independent values of the $2S_{1/2} - 8D_{5/2}$ interval which are obtained are in very good agreement (see table 1). For hydrogen, the average value of these data is: $\nu(2S_{1/2}-8D_{5/2}) = 770\ 649\ 561.5811(59)$ kHz. A similar procedure gives for deuterium: $\nu(2S_{1/2} - 8D_{5/2}) = 770\ 859\ 252.8483(55)$ kHz. These values are slightly different from the ones published in reference [47], mainly because of the recent measurement of the CO_2/OsO_4 laser. In addition to the uncertainties quoted

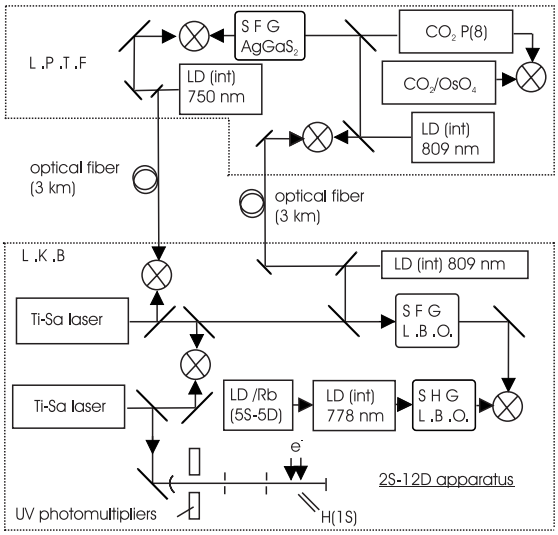

Fig. 11. Outline of the frequency chain between the $2S-12D$ hydrogen frequencies and the LD/Rb and CO_2/OsO_4 standards. The details are explained in the text (Ti-Sa: titanium sapphire laser, LD/Rb: rubidium stabilized laser diode, LD(int): intermediate laser diode, CO_2/OsO_4: osmium tetraoxyde stabilized CO_2 laser, SHG: second harmonic generation, SFG: sum frequency generation)

in the table, the final uncertainties take into account the second order Doppler effect (1 kHz), the measurement and the long term stability of the LD/Rb standard laser (2 kHz) and the imperfections of the theoretical model (4.5 kHz). With respect to reference [47], the uncertainties are also slightly more conservative.

In order to test the measurements of the $2S-8S$ and $2S-8D$ transitions, the frequencies of the $2S-12D$ intervals have also been measured in Paris [49]. This transition yields complementary information, because the $12D$ levels are very sensitive to stray electric fields (the quadratic Stark shift varies as n^7), and thus such a measurement provides a stringent test of Stark corrections to the Rydberg levels. The frequency difference between the $2S-12D$ transitions ($\lambda \approx 750$ nm, $\nu \approx 399.5$ THz) and the LD/Rb standard laser is about 14.2 THz, *i.e.* half of the frequency of the CO_2/OsO_4 standard. This frequency difference is bisected with an optical divider [56] (see Fig. 5). The frequency chain (see Fig. 11) is split between the LPTF and the LKB: the two optical fibers are used to transfer the CO_2/OsO_4 standard from the LPTF to the LKB, where the hydrogen transitions are observed. This chain includes an auxiliary source at 809 nm ($\nu \approx 370.5$ THz) such that the laser frequencies satisfy the equations:

$$\nu(2S-12D) + \nu(809) = 2\nu(LD/Rb)$$
$$\nu(2S-12D) - \nu(809) = \nu(CO_2)$$

The first equation is realized at the LKB while the second one is carried out at the LPTF. A first titanium-sapphire laser excites the hydrogen transition. A laser diode (power of 50 mW) is injected by the LD/Rb standard and frequency doubled in a LiB_3O_5 (LBO) crystal placed in a ring cavity. The generated UV beam is frequency compared to the frequency sum (made also in a LBO crystal) of the 750 and 809 nm radiations produced by a second titanium-sapphire laser and a laser diode. A part of the 809 nm source is sent via one fiber to the LPTF. There, a 809 nm local laser diode is phase locked to the one at LKB. A frequency sum of this 809 nm laser diode and of an intermediate CO_2 laser in an $AgGaS_2$ crystal produces a wave at 750 nm. This wave is used to phase lock, with a frequency shift δ, a laser diode at 750 nm which is sent back to the LKB by the second optical fiber. This 750 nm laser diode is frequency shifted by $\nu(CO_2)+\delta$ with respect to the one at 809 nm. In such a way, the two equations are simultaneously satisfied and all the frequency countings are performed in the LKB. Finally, the residual difference between the two titanium-sapphire lasers is measured with a fast photodiode or a Schottky diode.

The two $2S_{1/2}(F=1,3/2)-12D_{3/2}$ and $2S_{1/2}(F=1,3/2)-12D_{5/2}$ two-photon transitions have been measured in hydrogen and deuterium. For these transitions, the corrections due to the black body radiation and to the Stark effect are not negligible but amount to several kHz, especially the Stark correction of the $2S_{1/2}-12D_{3/2}$ (6 kHz). With the same analysis as for the $2S-8S/D$ transitions, the frequencies of the $2S_{1/2}-12D_{5/2}$ interval are derived to be $\nu(2S_{1/2}-12D_{5/2}) = 799\ 191\ 727.4028(67)$ MHz in hydrogen and $\nu(2S_{1/2}-12D_{5/2}) = 799\ 409\ 184.9676(65)$ MHz in deuterium. Ultimately, these measurements are slightly less precise than those for the $2S-8S/D$ transitions, owing to the smaller signal-to-noise ratio and the larger Stark shifts.

3.3 Comparison of the $1S-3S$ and $2S-6S/D$ Transitions

The experimental set-up on the $2S-nS/D$ transitions has also been used in Paris to deduce the Lamb shift of the $1S$ level via a comparison of the frequencies of the $1S-3S$ and $2S-6S/D$ transitions [57]. The principle of this experiment is similar to the ones made at Garching and at Yale, where the $1S-2S$ frequency was compared to the $2S-4S$, $2S-4P$ or $2S-4D$ frequencies [23,58]. In the Bohr model, these frequencies lie exactly in a ratio 4:1, and the deviation from this factor is mainly due to the Lamb shifts which vary as $1/n^3$.

Figure 12 shows the general scheme of the experiment. The same titanium-sapphire laser is used to observe, alternatively, the $2S-6S$ or $2S-6D$ transitions at 820 nm and the $1S-3S$ transition at 205 nm. The UV radiation at 205 nm is obtained from two successive doubling stages with a LBO crystal and a β-barium borate (BBO) crystal which are placed inside two enhancement cavities [59,60]. The first frequency doubling produces up to 500 mW at 410 nm for a pump power of 2.3 W at 820 nm. The second harmonic generation at 205 nm is far more challenging and provides a UV power of about 1 mW. To reduce the transit time broadening the $1S-3S$ transition is observed with an effusive

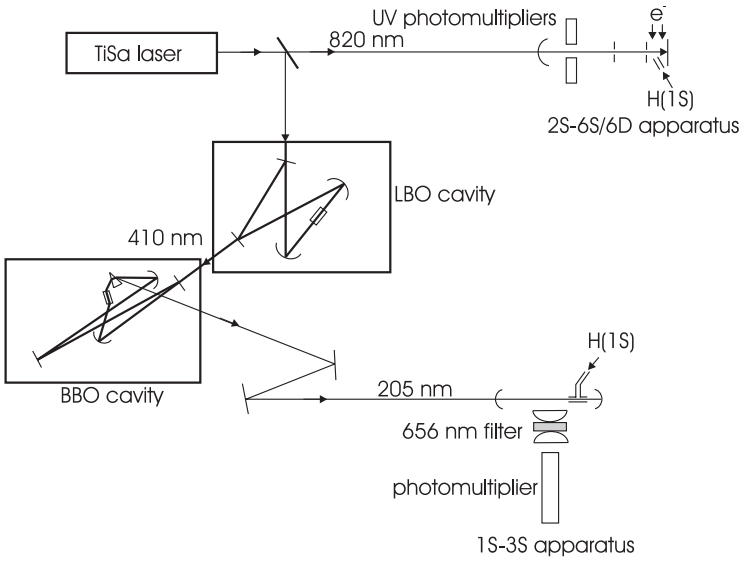

Fig. 12. Experimental setup for the frequency comparison between the $1S-3S$ and $2S-6S/D$ transitions (TiSa: titanium sapphire laser, LBO: lithium tri-borate crystal, BBO: β-barium borate crystal)

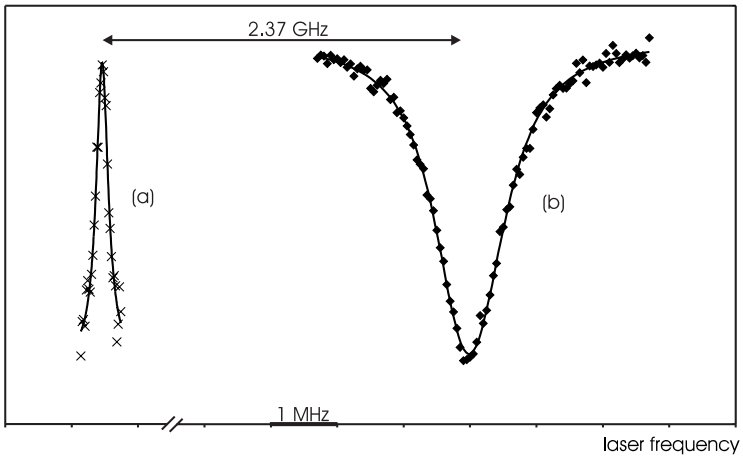

Fig. 13. Hydrogen two-photon spectra. a) $1S_{1/2}(F=1)-3S_{1/2}(F=1)$ transition. b) $2S_{1/2}(F=1)-6D_{5/2}$ transition. The two signals are shifted by about 2.37 GHz in terms of the laser frequency at 820 nm

atomic beam collinear with the UV beams. To increase the two-photon absorption probability, this atomic beam is also surrounded by a buildup cavity. The

two-photon transition is detected by monitoring the Balmer-α fluorescence due to the radiative decay $3S - 2P$.

The $1S_{1/2} - 3S_{1/2}$ frequency has been compared with those of the $2S_{1/2} - 6D_{5/2}$ and $2S_{1/2} - 6S_{1/2}$ transitions. Figure 13 shows, on the same frequency scale, the recordings of the $1S_{1/2} - 3S_{1/2}$ and $2S_{1/2} - 6D_{5/2}$ lines. As the $2S - 6S/D$ linewidth is larger than the $1S - 3S$ one, the accuracy is mainly limited by the uncertainty in the $2S - 6S/D$ line positions. Taking into account the results of these two measurements, one obtains for this frequency comparison $\nu(2S_{1/2} - 6D_{5/2}) - \frac{1}{4}\nu(1S - 3S) = 4\,699.1006(98)$ MHz.

4 Determination of the Rydberg Constant and Lamb Shifts

The aim of this section is to extract from the measurements the values of the Rydberg constant and Lamb shifts. This analysis is detailed in the references [50,61]. More details on the theory of atomic hydrogen can be found in several review articles [62,63,34]. It is convenient to express the energy levels in hydrogen as the sum of three terms: the first is the well known hyperfine interaction. The second, given by the Dirac equation for a particle with the reduced mass and by the first relativistic correction due to the recoil of the proton, is known exactly, apart from the uncertainties in the physical constants involved (mainly the Rydberg constant R_∞). The third term is the Lamb shift, which contains all the other corrections, *i.e.* the QED corrections, the other relativistic corrections due to the proton recoil and the effect of the proton charge distribution. Consequently, to extract R_∞ from the accurate measurements one needs to know the Lamb shifts. For this analysis, the theoretical values of the Lamb shifts are sufficiently precise, except for those of the $1S$ and $2S$ levels.

4.1 Rydberg Constant

Most of the combinations to derive R_∞, which scales all atomic energy levels and is used to adjust other constants [61], and the ground state Lamb shift $L(1S)$, which allows one of the best tests of QED, yield a comparable accuracy. Therefore, a general adjustment gives the best answers to date [61,49].

In hydrogen, there are several precise determinations of the $2S_{1/2} - 2P_{1/2}$ splitting by microwave spectroscopy [64,65] and by the anisotropy method [66]. Using the mean value of these results (1 057.8454(65) MHz), one can extract R_∞ from the $2S - nD$ measurements. The first part of table 2 gives the values of the Rydberg constant deduced from the $2S_{1/2} - 8D_{5/2}$ and $2S_{1/2} - 12D_{5/2}$ measurements in hydrogen. These two values have a similar precision and are in an acceptable agreement (they differ by about 1 standard deviation). Table 2 gives the average of these results ($R_\infty = 109\,737.315\,6855(11)$ cm^{-1}). The relative uncertainty (about 10^{-11}) comes from the optical frequency measurements (6.1×10^{-12}), the $2S_{1/2}$ Lamb shift (8.3×10^{-12}) and the proton-to-electron mass ratio (1.2×10^{-12}). The uncertainty due to the fine structure constant is

Table 2. Determination of the Rydberg constant

Method and transitions involved	$(R_\infty - 109737)$ cm^{-1}
Determination of R_∞ from the $2S-nD$ and $2S-2P$ measurements	
$2S-2P$ and $2S-8S/D$ in hydrogen	0.315 6861(13)
$2S-2P$ and $2S-12D$ in hydrogen	0.315 6848(13)
$2S-2P$, $2S-8S/D$ and $2S-12D$ in hydrogen	0.315 6855(11)
Determination of R_∞ from linear combination of optical frequencies measurements	
$2S-8S/D$, $1S-2S$ and $1/n^3$ law in hydrogen	0.315 6865(16)
$2S-12D$, $1S-2S$ and $1/n^3$ law in hydrogen	0.315 6842(17)
$2S-8S/D$, $2S-12D$, $1S-2S$ and $1/n^3$ law in hydrogen	0.315 6854(13)
$2S-8S/D$, $2S-12D$, $1S-2S$ and $1/n^3$ law in deuterium	0.315 6854(12)
$2S-8S/D$, $2S-12D$, $1S-2S$ and $1/n^3$ law in hydrogen and deuterium	0.315 6854(10)
General least squares adjustment in hydrogen and deuterium	
$2S-2P$, $2S-8S/D$, $2S-12D$, $1S-2S$ and $1/n^3$ law	0.315 685 50(84)

negligible (1.3×10^{-13}). This result is most precise if we don't make theoretical assumptions concerning the $1S_{1/2}$ and the $2S_{1/2}$ Lamb shifts. Unfortunately, this method is not appropriate for deuterium, because, for this isotope, no comparably accurate determination of the $2S_{1/2}$ Lamb shift has been performed.

Figure 14 compares the recent determinations of the Rydberg constant and shows the different steps of this improvement since 1986 (references in chronological order: [67,68,69,70,21,22,10,24,45,46,47,49,61,28]).

The other methods to determine R_∞ uses the $1/n^3$ scaling law of the Lamb shift which allows the accurate calculation of $L(1S)-n^3L(nS)$ [71]. Then we can form the linear combination of the $1S_{1/2}-2S_{1/2}$ and $2S_{1/2}-nD_{5/2}$ frequencies:

$$7\nu_H(2S_{1/2}-nD_{5/2})-\nu_H(1S_{1/2}-2S_{1/2})$$

where the quantity $L(1S)-8L(2S)$ appears. This method is independent of the microwave measurements of the $2S$ Lamb shift and is relevant for both hydrogen and deuterium. The results are given in the second part of table 2. The values obtained for hydrogen and deuterium are in perfect agreement. If we use all the precise optical frequency measurements in hydrogen and deuterium (transitions $1S_{1/2}-2S_{1/2}$, $2S_{1/2}-8D_{5/2}$ and $2S_{1/2}-12D_{5/2}$), we obtain a value of R_∞ more precise than the previous ones (R_∞ = 109 737.315 6854(10) cm^{-1}). This value is also in perfect agreement with the one deduced via the measurements of the $2S_{1/2}$ Lamb shift.

As already mentioned in the second part of this review, we made an average of these different determinations of R_∞ by performing a least squares adjustment [72] which takes into account all the precise experiments: the measurements of the $2S_{1/2}$ Lamb shift, the optical frequency measurements of the $1S-2S$ and $2S-nD$ transitions in hydrogen and deuterium, and also the measurements of

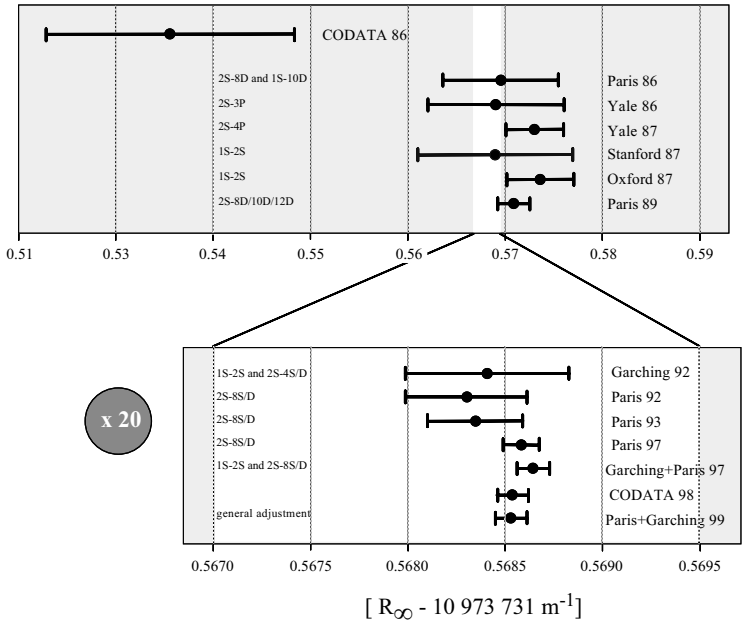

Fig. 14. A history of measurements of the Rydberg constant

the $1S$ Lamb shift [57,23,58]. The result ($R_\infty = 109\,737.315\,685\,50(84)\ \mathrm{cm}^{-1}$) is similar to the one of the 1998 adjustment of the fundamental constants [61], with a relative uncertainty of 7.7×10^{-12}. By comparison with the 1986 adjustment [67], the uncertainty is reduced by a factor of about 150.

4.2 Lamb Shifts

The first part of table 3 gives the determinations of the $1S$ Lamb shift obtained by comparison of the $1S-2S$ and $2S-4S/D$ or $2S-4P$ frequencies [23,58] or of the $1S-3S$ and $2S-6S/D$ frequencies [57]. The three results have a similar precision and are in good agreement.

Another way to obtain the $1S_{1/2}$ Lamb shift is to use the precise optical frequency measurements of the $1S_{1/2}-2S_{1/2}$ and $2S_{1/2}-nD_{5/2}$ transitions. A first method uses the experimental value of the $2S_{1/2}$ Lamb shift to extract R_∞ from the $2S_{1/2}-nD_{5/2}$ splitting (see the first part of table 2). Then the $1S_{1/2}$ Lamb shift is deduced from the $1S_{1/2}-2S_{1/2}$ frequency. The results are given in the second part of table 3. The final result ($L_H(1S_{1/2}) = 8\,172.840(31)$ MHz) is more precise than the precedent ones because of the very high accuracy of the optical frequency measurements. The 31 kHz uncertainty is due to the optical frequency measurements (15 kHz) and to the measurement of the $2S_{1/2}$ Lamb shift (27 kHz). In a second method, we can avoid this limitation by using the $1/n^3$ scaling law of the Lamb shift. The values obtained this way are slightly

Table 3. Determination of the $1S_{1/2}$ Lamb shift in hydrogen

Method and transitions involved	$L_H(1S_{1/2})$ (MHz)
Comparison of transition frequencies lying in a ratio 4:1	
$2S-2P$, $1S-3S$ and $2S-6S/D$	8172.825(47)
$2S-2P$, $1S-2S$ and $2S-4S/D$	8172.878(51)
$2S-2P$, $1S-2S$ and $2S-4P$	8172.834(48)
Comparison of the $1S-2S$ and $2S-nD$ frequencies using the $2S_{1/2}$ Lamb shift	
$2S-2P$, $1S-2S$ and $2S-8S/D$	8172.854(33)
$2S-2P$, $1S-2S$ and $2S-12D$	8172.825(34)
$2S-2P$, $1S-2S$, $2S-8S/D$ and $2S-12D$	8172.840(31)
Comparison of the $1S-2S$ and $2S-nD$ frequencies using the $1/n^3$ scaling law	
$2S-8S/D$, $2S-12D$, $1S-2S$ and $1/n^3$ law in hydrogen	8172.837(32)
$2S-8S/D$, $2S-12D$, $1S-2S$ and $1/n^3$ law in hydrogen and deuterium	8172.837(26)
General least squares adjustment in hydrogen and deuterium	
$2S-2P$, $2S-8S/D$, $2S-12D$, $1S-2S$ and $1/n^3$ law	8172.840(22)
Theory $r_p = 0.862(12)$ fm [74]	8172.816(34)
Theory $r_p = 0.805(11)$ fm [74]	8172.667(30)

more precise (see the third part of table 3). Moreover, this method provides us with the $2S_{1/2}$ Lamb shift and is reliable in the case of deuterium. The results are: $L_H(2S_{1/2}-2P_{1/2}) = 1\,057.8447(34)$ MHz in hydrogen, $L_D(1S_{1/2}) = 8\,183.967(26)$ MHz and $L_D(2S_{1/2}-2P_{1/2}) = 1\,059.2338(34)$ MHz in deuterium. These results for the $2S_{1/2}$ Lamb shift are independent and more precise than the direct determinations made by microwave spectroscopy.

Finally, with $L_H(1S_{1/2}) = 8\,172.840(22)$ MHz we give the result of the general adjustment with a relative uncertainty of 2.7×10^{-6}. This experimental value is in good agreement with theoretical predictions of the Lamb shift, if we assume the Mainz value for the proton charge radius ($r_p = 0.862(12)$ fm [73]) and include recent results for quantum electrodynamic two-loop contributions given by K. Pachucki [74]. These calculations gave a surprisingly large value for some higher order corrections. The agreement between theory and experiment lessens, if we assume the Stanford value for the proton charge radius ($r_p = 0.805(11)$ fm [75]). Let us remark, that S.G. Karshenboim has recently reanalyzed measurements of the proton charge radius, and obtained the value of 0.88(3) fm [76]. Conversely, if we believe the calculations of Ref. [74], we can deduce the radius of the proton charge distribution $r_p = 0.871(9)$ fm.

5 Conclusion and Prospects

The precision of the Rydberg constant and Lamb shifts is now limited by the uncertainties in the $2S-nS/D$ frequencies in hydrogen, which, in the Paris ex-

periment, are mainly caused by light shifts. To obtain more accurate values of these frequencies, a first possibility is to use ultracold hydrogen to increase the interaction time and decrease the light shifts [77]. In Paris, we intend to measure the optical frequency of the $1S-3S$ transition. In this case, as the number of atoms in the 1S atomic beam is about 10^8 times larger than in the metastable atomic beam, we can observe the transition with a very small light power and, consequently, with negligible light shifts. For this experiment, we plan to compensate the second order Doppler effect using a magnetic field perpendicular to the atomic beam [78,79].

In Garching, we are planning to measure the absolute frequency of the hydrogen $1S-2S$ transition with an accuracy of a few parts in 10^{15} in the near future. Although precise spectroscopy of the hydrogen atom has been pursued for more than a century, advances in experimental technology promise dramatic further advances. The art of laser frequency stabilization has been perfected so that coherent optical sources of Hertz or sub-Hertz linewidth are now reality [80,81]. Magnetically trapped cold hydrogen atoms [82] may eventually permit atomic fountain experiments [83,84] that could approach the 1.3 Hz natural linewidth of the hydrogen $1S-2S$ transition.

Continuous wave coherent Lyman-α radiation has recently become available [85] so that laser cooling or sensitive shelving spectroscopy of magnetically trapped hydrogen atoms is coming within reach. The ability to work with a small number of atoms is of particular interest for laser spectroscopy of antihydrogen, a goal pursued by the ATRAP and ATHENA collaborations at CERN [8].

Lamb shift measurements on muonic hydrogen, as now pursued with a novel intense source of slow muons at the Paul Scherrer Institute [86,87] promise to yield an accurate rms charge radius of the proton, so that bound state QED can be tested to new levels of scrutiny.

These experimental advances are inspiring renewed theoretical efforts to calculate higher order QED corrections, as discussed elsewhere in these Proceedings.

The work in Paris was partially supported by the Bureau National de Métrologie, by the Direction des Recherches et Etudes Techniques and by the European Community (SCIENCE cooperation Contract No. SCI*-CT92-0816 and network Contract No. CHRX-CT93-0105).

References

1. G.W. Series and T.W. Hänsch: 'Optical Spectroscopy'. In: *The Spectrum of Atomic Hydrogen: Advances*, ed. by G.W. Series (World Scientific Publishing Co. 1988), pp. 293–330
2. T.W. Hänsch, A.L. Schawlow, and G.W. Series: Scientific American **240**, 94 (1979)
3. T.W. Hänsch: 'High Resolution Spectroscopy of Hydrogen'. In: *The Hydrogen Atom*, ed. by G.F. Bassani, M. Inguscio, and T.W. Hänsch (Springer, Berlin Heidelberg 1989), pp. 93–102
4. M. Kourogi, B. Widiyatomoko, Y. Takeuchi, and M. Ohtsu: IEEE J. Quantum Electron. **31**, 2120 (1995)
5. L. Brothers, D. Lee, and N. Wong: Opt. Lett. **19**, 245 (1994)

6. Th. Udem, J. Reichert, R. Holzwarth, S. Diddams, D. Jones, J. Ye, S. Cundiff, T.W. Hänsch, and J.L. Hall: *this book*, pp. 125–144
7. P.J. Mohr and B.N. Taylor: *this book*, pp. 145–156
8. J. Walz, A. Pahl, K.S.E. Eikema, and T.W. Hänsch: *this edition*, pp. 521–527
9. C. Zimmermann, R. Kallenbach, and T.W. Hänsch: Phys. Rev. Lett. **65**, 571 (1990)
10. F. Biraben, J.C. Garreau, L. Julien, and M. Allegrini: Phys. Rev. Lett. **62**, 621 (1989)
11. R.L. Walsworth, Jr., I.F. Silvera, H.P. Godfried, and C.C. Agosta: Phys. Rev. A **34**, 2550 (1986)
12. M.D. Hürlimann, W.N Hardy, A.J. Berlinsky, and R.W. Cline: Phys. Rev. A. **34**, 1605 (1986)
13. A. Huber, B. Gross, M. Weitz, and T.W. Hänsch: Phys. Rev. A **59**, 1844 (1999)
14. F. Schmidt-Kaler, D. Leibfried, S. Seel, C. Zimmermann, W. König, M. Weitz, and T.W. Hänsch: Phys. Rev. A **51**, 2789 (1995)
15. J. Hought, D. Hils, M.D. Rayman, Ma L.-S., L. Hollberg, and J.L. Hall: Appl. Phys. B **33**, 179 (1984); R.W. Drewer, J. Hough, G.M. Ford, A.J. Munley, and H. Ward: *ibid.* **31**, 97 (1983)
16. T.W. Hänsch and B. Couillaud: Opt. Commun. **35**, 441 (1980)
17. J.C. Garreau, M. Allegrini, L. Julien, and F. Biraben: J. Phys. France **51**, 2263 (1990)
18. J.C. Garreau, M. Allegrini, L. Julien, and F. Biraben: J. Phys. France **51**, 2275 (1990)
19. J.C. Garreau, M. Allegrini, L. Julien, and F. Biraben: J. Phys. France **51**, 2293 (1990)
20. M. Weitz, F. Schmidt-Kaler, and T.W. Hänsch: Phys. Rev. Lett. **68**, 1120 (1992)
21. D.H. McIntyre, R.G. Beausoleil, C.J. Foot, E.A. Hildum, B. Couillaud, and T.W. Hänsch: Phys. Rev. A **39**, 4591 (1989)
22. M.G. Boshier, P.E.G. Baird, C.J. Foot, E.A. Hinds, M.D. Plimmer, D.N. Stacey, J.B. Swan, D.A. Tate, D.M. Warrington, and G.K. Woodgate: Nature **330**, 463 (1987); Phys. Rev. A **40**, 6169 (1989)
23. M. Weitz, A. Huber, F. Schmidt-Kaler, D. Leibfried, and T.W. Hänsch: Phys. Rev. Lett. **72**, 328 (1994)
24. T. Andreae, W. König, R. Wynands, D. Leibfried, F. Schmidt-Kaler, C. Zimmermann, D. Meschede, and T.W. Hänsch: Phys. Rev. Lett. **69**, 1923 (1992)
25. H. Schnatz, B. Lipphardt, J. Helmcke, F. Riehle, and G. Zinner: Phys. Rev. Lett. **76**, 18 (1995)
26. D. Leibfried, F. Schmidt-Kaler, M. Weitz, and T.W. Hänsch: Appl. Phys. B **56**, 65 (1993)
27. Th. Udem, A. Huber, B. Gross, J. Reichert, M. Prevedelli, M. Weitz, and T.W. Hänsch: Phys. Rev. Lett. **79**, 2646 (1997)
28. M. Niering, R. Holzwarth, J. Reichert, P. Pokasov, Th. Udem, M. Weitz, T.W. Hänsch, P. Lemonde, G. Santarelli, M. Abgrall, P. Laurent, C. Salomon, and A. Clairon: Phys. Rev. Lett. **84**, 5496 (2000)
29. J. Reichert, M. Niering, R. Holzwarth, M. Weitz, Th. Udem, and T.W. Hänsch: Phys. Rev. Lett. **84**, 3232 (2000)
30. P. Lemonde, P. Laurent, G. Santarelli, M. Abgrall, Y. Sortais, S. Bize, C. Nicolas, S. Zhang, A. Clairon, N. Dimarcq, P. Petit, A. Mann, A. Luiten, S. Chang, and C. Salomon: 'Cold Atom Clocks on Earth and in Space'. In: *Frequency Measurement and Control*, ed. by A.N. Luiten (Springer, Berlin, Heidelberg 2000), pp. 131–153

31. F. Schmidt-Kaler, D. Leibfried, M. Weitz, and T.W. Hänsch: Phys. Rev. Lett. **70**, 2261 (1993)
32. A. Huber, Th. Udem, B. Gross, J. Reichert, M. Kourogi, K. Pachucki, M. Weitz, and T.W. Hänsch: Phys. Rev. Lett. **80**, 468 (1998)
33. K. Imai, M. Kourogi, and M. Ohtsu: IEEE Journal of Quantum Electronics. **34**, 54 (1998)
34. K. Pachucki, D. Leibfried, M. Weitz, A. Huber, W. König, and T.W. Hänsch: J. Phys. B **29**, 177 (1996)
35. A higher order correction [36] is added to the number previously given in Ref. [32] and the uncertainty is now dominated by two sources: the electron proton mass ratio (1.5 kHz) [37] and higher order deuteron structure effects (0.5 kHz).
36. K. Pachucki, and S.G. Karshenboim: Phys. Rev. A **60**, 2792 (1999)
37. D.L. Farnham, R.S Van Dyck, and P.B. Schwinberg: Phys. Rev. Lett. **75**, 3598 (1995)
38. A.J. Buchmann, H. Henning, and P.U. Sauer: Few-Body Systems **21**, 149 (1996)
39. S. Kopecky, P. Riehs, J.A. Harvey, and N.W. Hill: Phys. Rev. Lett. **74**, 2427 (1995)
40. S.K. Klarsfeld, J. Martorell, J.A. Oteo, M. Nishimura, and D.W. Sprung: Nucl. Phys. A **456**, 373 (1986)
41. R.W. Berard, F.R. Buskirk, E.B. Dally, J.N. Dyer, X.K. Maruyama, R.L. Topping, and T.J. Traverso: Phys. Lett. B **47**, 355 (1973)
42. G.G. Simon, Ch. Schmitt., and V.H. Walther: Nucl. Phys. A **456**, 373 (1986)
43. I. Sick and D. Trautmann: Phys. Lett. B **375**, 16 (1996)
44. M. Allegrini, F. Biraben, B. Cagnac, J.C. Garreau, and L. Julien: In *The Hydrogen Atom*, ed. by G.F. Bassani, M. Inguscio, and T.W. Hänsch (Springer, Berlin Heidelberg 1989) pp. 49–60
45. F. Nez, M.D. Plimmer, S. Bourzeix, L. Julien, F. Biraben, R. Felder, O. Acef, J.J. Zondy, P. Laurent, A. Clairon, M. Abed, Y. Millerioux, and P. Juncar: Phys. Rev. Lett. **69**, 2326 (1992)
46. F. Nez, M.D. Plimmer, S. Bourzeix, L. Julien, F. Biraben, R. Felder, Y. Millerioux, and P. de Natale: Europhys. Lett. **24**, 635 (1993)
47. B. de Beauvoir, F. Nez, L. Julien, B. Cagnac, F. Biraben, D. Touahri, L. Hilico, O. Acef, A. Clairon, and J.J. Zondy: Phys. Rev. Lett. **78**, 440 (1997)
48. D. Touahri, O. Acef, A. Clairon, J.J. Zondy, R. Felder, L. Hilico, B. de Beauvoir, F. Biraben, and F. Nez: Opt. Commun. **133**, 471 (1997)
49. C. Schwob, L. Jozefowski, B. de Beauvoir, L. Hilico, F. Nez, L. Julien, F. Biraben, O. Acef, and A. Clairon: Phys. Rev. Lett. **82**, 4960 (1999)
50. B. de Beauvoir, C. Schwob, O. Acef, L. Jozefowski, L. Hilico, F. Nez, L. Julien, A. Clairon, and F. Biraben: Eur. Phys. J. D **12**, 61 (2000)
51. F. Nez, F. Biraben, R. Felder, and Y. Millerioux: Opt. Commun. **102**, 432 (1993)
52. Y Millerioux, D. Touahri, L. Hilico, A. Clairon, R. Felder, F. Biraben, and B. de Beauvoir: Opt. Commun. **103**, 91 (1994)
53. L. Hilico, R. Felder, D. Touahri, O. Acef, A. Clairon, and F. Biraben: Eur. Phys. J. AP **4**, 219 (1998)
54. B. de Beauvoir, F. Nez, L. Hilico, L. Julien, F. Biraben, B. Cagnac, J.J. Zondy, D. Touahri, O. Acef, and A. Clairon: Eur. Phys. J. D **1**, 227 (1998)
55. G.D. Rovera and O. Acef: IEEE Trans. Inst. Meas. **48,**571 (1999)
56. H.R. Telle, D. Meschede, and T.W. Hänsch: Opt. Lett. **15**, 532 (1990)
57. S. Bourzeix, B. de Beauvoir, F. Nez, M.D. Plimmer, F. de Tomasi, L. Julien, F. Biraben, and D.N. Stacey: Phys. Rev. Lett. **76**, 384 (1996)
58. D.J. Berkeland, E.A. Hinds, and M.G. Boshier: Phys. Rev. Lett. **75**, 2470 (1995)

59. S. Bourzeix, M.D. Plimmer, F. Nez, L. Julien, and F. Biraben: Opt. Commun. **99**, 89 (1993)
60. S. Bourzeix, B. de Beauvoir, F. Nez, F. de Tomasi, L. Julien, and F. Biraben: Opt. Commun. **133**, 239 (1997)
61. P.J. Mohr and B.N. Taylor: Rev. Mod. Phys. **72,** 351 (2000)
62. J.R. Sapirstein and D.R. Yennie: in *Quantum Electrodynamics*, edited by T. Kinoshita, World Scientific, Singapore (1990), pp. 560–672
63. P.J. Mohr: in *Atomic, Molecular & Optical Physics Handbook*, edited by G.W.F. Drake, AIP, New York (1996), pp. 341–352
64. S.R. Lundeen and F.M. Pipkin: Phys. Rev. Lett. **46**, 232 (1981)
65. E.W. Hagley and F.M. Pipkin: Phys. Rev. Lett. **72**, 1172 (1994)
66. A. van Wijngaarden, F. Holuj, and G.F.W. Drake: Can. J. Phys. **76**, 95 (1998)
67. E.R. Cohen and B.N. Taylor: Rev. Mod. Phys. **59**, 1121 (1987)
68. F. Biraben, J.C. Garreau, and L. Julien: Europhys. Lett. **2**, 925 (1986)
69. P. Zhao, W. Lichten, H.P. Layer, and J.C. Bergquist: Phys. Rev. A **34**, 5138 (1986)
70. P. Zhao, W. Lichten, H.P. Layer, and J.C. Bergquist: Phys. Rev. Lett. **58**, 1293 (1987)
71. S.G. Karshenboim: J. Phys. B **29**, L29 (1996); Z. Phys. D **39**, 109 (1997)
72. see e.g. E.R. Cohen, K.M. Crowe, and J.W.M. Dumond: 'The Fundamental Constants of Physics' (Interscience Publishers, Inc., New York 1957), pp. 222–246
73. G.G. Simon, C. Schmitt, F. Borkovski, and V.H. Walther: Nucl. Phys. A **333**, 381 (1980)
74. K. Pachucki. E-print archive: physics/0011044, submitted to Phys. Rev. A
75. L.N. Hand, D.J. Miller, and R. Wilson: Rev. Mod. Phys. **35**, 335 (1963)
76. S.G. Karshenboim: Can. J. Phys. **77**, 241 (1999); private communication
77. C.L. Cesar, D.G. Fried, T.C. Killian, A.D. Polcyn, J.C. Sandberg, I.A. Yu, T.J. Greytak, D. Kleppner, and J.M. Doyle: Phys. Rev. Lett. **77**, 255 (1996)
78. F. Biraben, L. Julien, J. Plon, and F. Nez: Europhys. Lett. **15**, 831 (1991)
79. G. Hagel, R. Battesti, C. Schwob, F. Nez, L. Julien, F. Biraben, O. Acef, J.J. Zondy, and A. Clairon: *this edition*, pp. 328–334
80. B.C. Young, F.C. Cruz, W.M. Itano, and J.C. Bergquist: Phys. Rev. Lett. **82**, 3799 (1999)
81. T. Becker, M. Eichenseer, A.Y. Nevsky, E. Peik, C. Schwedes, M.N. Skvortsov, J. v. Zanthier, and H. Walther: *this edition*, pp. 545–553
82. D.G. Fried, T.C. Killian, L. Willmann, D. Landhuis, S.C. Moss, D. Kleppner, and T.J. Greytak: Phys. Rev. Lett. **81**, 3811 (1998)
83. R.G. Beausoleil and T.W. Hänsch: Opt. Lett. **10**, 547 (1985)
84. R.G. Beausoleil and T.W. Hänsch: Phys. Rev. A **33**, 1661 (1986)
85. K.S.E. Eikema, J. Walz, and T.W. Hänsch, Phys. Rev. Lett. **83**, 3828 (1999)
86. R. Pohl, F. Biraben, C.A.N. Conde, C. Donche-Gay, T.W. Hänsch, F.J. Hartmann, P. Hauser, V.W. Hughes, O. Huot, P. Indelicato, P. Knowles, F. Kottmann, Y.-W. Liu, V.E. Markushin, F. Mulhauser, F. Nez, C. Petitjean, P. Rabinowitz, J.M.F. dos Santos, L.A. Schaller, H. Schneuwly, W. Schott, D. Taqqu, and J.F.C.A. Veloso: *this edition*, pp. 454–466
87. D. Taqqu, F. Biraben, C.A.N. Conde, T.W. Hänsch, F.J. Hartmann, P. Hauser, P. Indelicato, P. Knowles, F. Kottmann, F. Mulhauser, C. Petitjean, R. Pohl, P. Rabinowitz, R. Rosenfelder, J.M.F. Santos, W. Schott, L.M. Simons, and J. Veloso: Hyperfine Interact. **119**, 311 (1999)